IEEE Access
Multidisciplinary | Rapid Review | Open Access Journal

Received January 28, 2021, accepted February 23, 2021, date of publication March 12, 2021, date of current version March 23, 2021.

Digital Object Identifier 10.1109/ACCESS.2021.3065745

Digital Predistortion in High Throughput Satellites: Architectures and Performance

OVAIS BIN USMAN, (Member, IEEE), AND ANDREAS KNOPP, (Senior Member, IEEE)
Chair of Signal Processing, Bundeswehr University Munich, 85579 Neubiberg, Germany

Corresponding author: Ovais Bin Usman (ovais.usman@unibw.de)

This work was supported by the German Aerospace Centre (DLR), Space Administration, under Grant 50YB1714.

ABSTRACT The future of satellites lies in the deployment of high throughput satellites (HTS). Moreover, HTS will also play an important role in the up coming 5G mobile networks where HTS will provide services like disaster relief, remote automation, maritime services etc. However, the distortions caused by the on-board transponder filters and high power amplifiers (HPAs) reduce the overall performance of HTS. To increase the power and bandwidth efficiency, the transponder HPAs are often operated close to saturation and in multicarrier mode. In addition, the transponder filters are built with tighter guard bands to minimize the out-of-band (OOB) radiations. Such operation conditions introduce severe linear and non-linear distortions in the transponder's output in terms of inter-modulation (IMD) noise, spectral regrowth, and memory effects. Digital predistortion (DPD) can effectively mitigate these distortions. This article proposes an on-board implementation of a ground-based state-of-the-art bandlimited memory polynomial (MP) DPD method to mitigate the aforementioned distortions. The authors stress on the fact that the on-board application of the proposed ground-based DPD makes it the most suitable DPD method for HTS. However, the focus of this article lies in the identification of the system parameters which effect the predistortion performance. To this end, the performance of the considered state-of-the-art DPD is thoroughly analyzed for varying uplink-signal, transponder and DPD specific parameters.

INDEX TERMS Bandlimited predistortion, digital predistortion (DPD), high power amplifiers (HPAs), high throughput satellites (HTS), non-linear distortions, on-board processors (OBPs), parameter identification.

I. INTRODUCTION

Today the satellite industry is moving from a broadcast to a unicast paradigm. This has led to an extensive use of high throughput satellites (HTS). HTS in combination with multi-beam architectures aim to deliver high speed broadband services such as Video-on-Demand. In addition, HTS will also be incorporated in the coming fifth generation (5G) of mobile communications [1]. Furthermore, the growing demand for flexible payloads in HTS has led to the emergence of transparent (bent pipe) payload architectures with on-board signal processing capabilities [2].

Distortions caused by the physical components on-board the satellites, especially by the payload's high power amplifiers (HPAs) [3] and the input/output multiplexing (IMUX/OMUX) filters [4], reduce the overall performance of the HTS. HPAs are an integral part of the payload [5], [6]. They are inherently non-linear power hungry devices, and can consume up to 70% of the system energy [7]. Since power is a limited resource in satellites, it should be utilized efficiently. Although operating HPAs close to saturation increases their power efficiency, it also introduces severe non-linear distortions. These distortions include non-linear inter-symbol interference (ISI), inter-modulation (IMD) distortion, and out-of-band (OOB) distortion, also known as spectral regrowth or spectral widening [5]–[7]. Non-linear ISI leads to the clustering and warping of the signal constellation (see Figure 1b). In current satellite systems, the multicarrier operation of the on-board HPAs is required to maximize the bandwidth efficiency [8]. This also keeps the total number of HPAs in the payload sufficiently low. A smaller number of the on-board HPAs leads to a reduced power consumption and a lower dry launch mass of the satellite. However, the multicarrier operation leads to severe inter-carrier-interference (ICI), adjacent channel interference (ACI) and memory effects, especially when the HPAs are operated in

The associate editor coordinating the review of this manuscript and approving it for publication was Tianhua Xu.

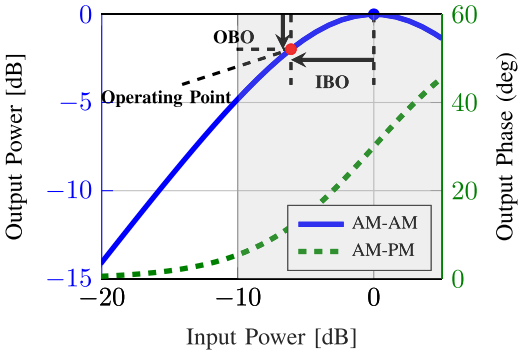

(a) Non-linear AM-AM and AM-PM for a typical PA

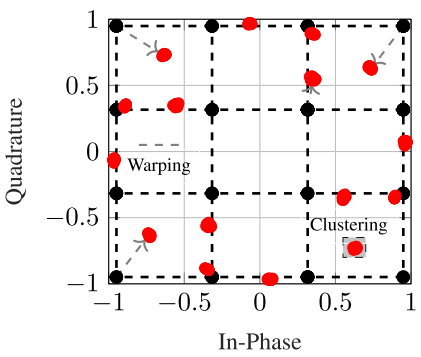

(b) Clustering and Warping effect

FIGURE 1. HPA and the associated non-linear characteristics.

wideband and close to saturation. In addition, the non-linear effects of HPAs become more significant when higher order modulation schemes are employed [9]. Apart from the distortions caused by the non-linear operation of HPAs, the memory effects introduced by the payload's IMUX and OMUX filters also account for a large portion of the overall distortion observed in a satellite channel [4]. The frequency dependent behavior of the IMUX and OMUX introduces linear and non-linear distortions. These distortions include ISI, clustering of the constellation points, and more importantly a variable phase shift in the spectral components of the downlink signal [4]. To maximize the bandwidth efficiency and to minimize OOB radiations, the OMUX filters are often designed with a tighter guard band (GB) compared to the IMUX filters. However, this leads to higher fluctuations in the group delay profile of the OMUX when compared to the IMUX group delay profile [10]. A tighter guard band introduces significant distortions in the edge carriers. Thus, in order to maintain a higher power and bandwidth efficiency, and to improve system performance, strategies to compensate for the distortions introduced by the HPAs and IMUX/OMUX are of interest.

Predistortion or equalization can be implemented to compensate the above mentioned distortions. The advantage of performing predistortion especially on-board the satellite lies in the fact that only a single predistorter is needed to mitigate the HPA non-linearity compared to emplyoing an equalizer at each user terminal [7]. A low complexity linear equalizer has been introduced in the DVB-S2X receiver [11]. However, the linear equalizer in [11] cannot mitigate the non-linear distortions and memory effects introduced by the HPAs. Therefore, complex solutions such as Volterra equalizers [12]–[14] are needed at the receiver to compensate for the non-linearities. However, such equalizers drastically increase the receiver's complexity. In addition, on-board predistortion can perform better than equalization due to the absence of downlink noise [6]. Predistortion can either be implemented on-ground at the gateway or on-board the satellite. In a typical HTS application scenario involving multiple gateways, implementing on-ground predistortion would require the knowledge of all the symbols or carriers at a centralized location on earth, which is not possible all the time. Hence, it is more feasible to implement predistortion on-board the satellite. Typically, an analog linearizer is built in the channel amplifier (CAMP) of the HPA [15]–[17]. However, due to their non-adaptive nature, the analog linearizers suffer from a graceful degradation in performance because of the variation in the HPA's non-linear characteristics induced by the changes in temperature and aging effects [18]. This pushes for the need of not only on-board but adaptive digital predistortion (DPD) solutions. Such solutions can be implemented using digital on-board processors (OBPs).

Due to the limitations like weight, power and radiation hardening requirements of the hardware in satellites, less powerful OBPs are employed on-board [19]. The current state-of-the-art OBPs lag in performance when compared to the digital signal processors (DSPs) employed in ground stations [20], [21]. To implement adaptive DPD solutions, a feedback loop is required. Conventionally, the bandwidth of the HPA output reaches up to five times that of the input signal bandwidth due to the spectral regrowth [19], [22]. Sampling such high bandwidth signals in the feedback path would imply using analog-to-digital converters (ADCs) and DSPs with ultra high sampling rates, which is currently not possible, and would consume a lot of power [23]. Therefore to perform adaptive on-board DPD, the bandwidth of the feedback path is restricted by an analog bandpass filter to allow the use of low sampling rate ADCs and DSPs [22]. Moreover, predistortion itself is a non-linear operation which results in bandwidth expansion of the input signal. However, the entire bandwidth of the predistorted output cannot be sampled back to the analog domain due to the unavailability of space grade digital-to-analog converters (DACs) with ultra-high sampling rates. As a result, for HTS DPD applications, a bandlimitation must be introduced in the forward path as well. Thus, this work focuses on on-board bandlimited DPD solutions for HTS.

Several parameters affect the DPD performance, ranging from the uplink-signal to transponder and DPD algorithm related parameters. To justify the on-board DPD implementation especially when using the power consuming OBPs, it is vital to identify the scenarios and parameters which maximize the DPD gain. Therefore, the primary focus of this article lies in performing a system parameter identification analysis for DPD to maximize the predistortion gain. Due to their low complexity and linear parameterization, the state-of-the-art memory polynomial [24] (MP)-based DPD solutions incorporating the in-direct learning architectures (IDLA) [3], [10] are considered in this work. A justification for implementing the DPD method presented in [10] is provided in Section III. The state-of-the-art bandlimited direct learning architecture (DLA)-based DPD algorithms [22], [25] are much more complex in nature, as they first require an HPA model estimation, and then the DPD coefficients are computed based on the estimated HPA model. Typically, the block-based DPD methods implementing DLA require two complex-matrix inversions per iteration. This would result in higher computing delays. Moreover, when implementing DLA-based DPD methods, the OBPs will consume more power, and require additional computing resources. An increased overall power consumption requirement translates into the additional solar panel array area which ultimately leads to a higher dry launch mass. DLA-based DPD methods are not in the scope of this work. The main contribution of the paper is to identify the system parameters which affect the DPD performance, and to perform a novel bandlimitation analysis. Different publications in the literature present novel algorithms to minimize the losses incurred due to the bandlimitation constraints for various simulated scenarios [10], [22], [26]. However, the focus of the bandlimitation analysis presented in this work is to find out how low the bandwidth in the critical feedback path can be with respect to the transmitted signal bandwidth to still achieve a gain when the considered state-of-the-art DPD method is implemented. To the authors best knowledge, no previously reported work answers this question, or discusses in depth the effect of system parameters on the DPD performance. Identifying the key parameters which effect the DPD performance can serve as a basis for the optimization of DPD algorithms to maximize their gain, and to facilitate their implementation in hardware platforms.

From this point on, the paper is organized as follows. The non-linear HPA models used in this work are presented in Section II. A complete overview of different classes and types of predistortion techniques is presented in Section III. In addition, the class and type of predistortion best suited for HTS is also proposed in Section III. The mathematical framework for the considered DPD method is provided in Section IV. The novel system parameter identification and bandlimitation analysis is presented in Section V. Lastly, conclusions are drawn in Section VI.

II. NON-LINEAR HPA MODELS

This section presents the analytical models of HPAs applied in this work to perform the system parameter identification analysis. HPA models can be classified as memoryless models or models with memory.

A. MEMORYLESS MODELS

Non-linear memoryless models are frequency independent, and are valid when HPAs operate in narrowband. The memoryless Saleh model [36] is extensively used in the literature to model power amplifiers (PAs) [37], [38], especially the travelling-wave-tube-amplifiers (TWTAs) which are typically employed in HTS payloads. Other memoryless models include the Rapp [39] and Ghorbani model [40]. However, these models are better suited for solid-state-power amplifiers (SSPAs). SSPAs are not common in HTS payloads due to their lower DC-to-RF conversion efficiency. In addition, the Rapp model does not cater for phase distortions of the HPAs. The AM-AM and AM-PM characteristics of the Saleh model are given as follows

$$g_{AM}\left(|x\left(t\right)|\right) = \frac{\alpha_{AM}\,|x\left(t\right)|}{1+\beta_{AM}\,|x\left(t\right)|^2}, \tag{1a}$$

$$\Phi_{PM}\left(|x\left(t\right)|\right) = \frac{\alpha_{PM}\,|x\left(t\right)|^2}{1+\beta_{PM}\,|x\left(t\right)|^2}. \tag{1b}$$

α_{AM}, α_{PM}, β_{AM} and β_{PM} are the four Saleh model coefficients. $g_{AM}\left(x\right)$ and $\Phi_{PM}\left(x\right)$ are the non-linear functions representing the AM-AM and AM-PM characteristics of the PA. $|x\left(t\right)|$ and $\varphi\left(x(t)\right)$ are magnitude and phase of the input signal $x(t)$. The resulting output of the PA for the Saleh model is given by (2).

$$y\left(t\right) = g_{AM}\left(x\left(t\right)\right)\cdot e^{j\{\varphi(x(t))+\Phi_{PM}(x(t))\}}. \tag{2}$$

B. MODELS WITH MEMORY

When HPAs are operated in wideband, their output exhibits memory effects. The memory polynomial (MP) model [24] is a simplified special case of the Volterra model [41], and it is often utilized for HPA modelling in wideband applications [3], [22], [42]. The MP model contains the diagonal Volterra kernels (coefficients) only [43], as a result, it exhibits low computational complexity. The input-output relationship of the MP model is given below.

$$y\left[n\right] = \sum_{q=0}^{Q-1}\sum_{k=1}^{K} w_{k,q}\cdot x\left[\text{n-q}\right]\cdot\left|x\left[\text{n-q}\right]\right|^{k-1}, \tag{3}$$

where $w_{k,q}$ are the MP coefficients. Q is the maximum memory depth, and K is the non-linearity order. MPs have linearly parameterized coefficients which makes the coefficient estimation process robust and low-effort.

III. LITERATURE OVERVIEW

This section details the different classes and types of predistorters existing in the literature. Moreover, the section also

TABLE 1. Classes of predistortion. IF: Intermediate frequency, BB: baseband, RF: radio frequency.

	Signal predistortion	Data predistortion
Performed on	pulse-shaped/uplink-signal	data symbols
Location	on-ground/on-board just before the PA	on-ground/on-board (regenerative payloads only)
Technology	digital/analog	digital
Frequency	IF(digital), BB (digital), RF (analog)	BB (digital)
Adaptive	digital: yes, analog: no	yes
References	[3], [19], [16], [18], [22]	[27], [28], [29]

TABLE 2. State-of-the-art predistortion techniques, and their suitability for HTS.

Technique	Class	Employment	Complexity	Features	Performance	References	Suited for HTS
Analog Cubic PD	Signal	on-ground on-board	Very low Complexity: 2 to 3 coefficients	**Non-adaptive Memoryless**	degrades with time	[16]	on-ground: wideband narrowband **on-board: wideband narrowband**
Look-up tables (LUT)	Signal Data	on-ground on-board	High Complexity: Size of LUT grows exponentially with memory depth and modulation order.	Adaptive Memory Memoryless	increases with the size of LUT	Data: [29] Signal: [30]	on-ground: wideband narrowband on-board: narrowband
Neural networks	Signal Data	on-ground on-board	Very high complexity: Extremely large number of DPD coefficients, especially in wideband	Adaptive Memory Memoryless	depends on the activation function	Signal: [31] [32], [33]	on-ground: wideband narrowband on-board: narrowband
Successive Interference Cancellation	Signal Data	on-ground on-board	Medium-high complexity, iteration dependent, HPA/OMUX model required, feed-forward approach	Adaptive Memory Memoryless Near optimal gain	increases with number of internal iterations	Data: [28] [4]	on-ground: wideband narrowband
Volterra:*p*th-order inverse	Signal	on-ground on-board	High complexity: Number of coefficients grow exponentially with order/memory, HPA model required	Adaptive Memory Memoryless	increases with memory and order	[34] [35] [9]	on-ground: wideband narrowband on-board: narrowband
Volterra: Memory Polynomials	Signal	on-ground on-board	Low-medium complexity MP: simplified form of Volterra, Direct and In-direct learning-based implementations	**Adaptive Memory** Memoryless	increases with optimal memory and order setting	In-direct: [3], [10] Direct: [22], [25]	on-ground: wideband narrowband **on-board: wideband narrowband**

proposes the on-board implementation of the ground-based bandlimited MP DPD, presented in [10], as the most suited DPD approach for HTS.

A. CLASSES OF PREDISTORTERS

Predistortion can be classified according to two main criteria. The type of signal which is modified before transmission (data or signal predistorters) and the applied technology (digital or analog predistorters). Table 1 lists these classes and some of their important characteristics.

B. PREDISTORTION TECHNIQUES

A variety of predistortion techniques exist within the different classes of predistortion presented in Table 1. Table 2 lists some of the state-of-the-art predistortion techniques, and their suitability for HTS. Although analog linearizers offer a cost effective solution especially at very high bandwidths [44], their non-adaptive and memoryless nature makes them an impractical standalone solution for HTS. Moreover, Beidas *et al.* in [28], [45] and Kelly *et al.* in [10] advocate for adaptive DPD solutions over the analog counterparts. Apart from the analog cubic predistorter, all the listed techniques in Table 2 are digital, and maintain their performance due to their adaptive nature. However, the accuracy and performance of each method depends on the technique related parameters. Table 2 suggests that the lookup table (LUT) [29], [30], neural network (NN) [31]–[33], and p-th order inverse-based [9], [34], [35] DPD methods are not practical for HTS as they exhibit high computational complexity, especially in wideband applications. These approaches require an extremely large number of DPD coefficients in the wideband operation on the account of higher memory effects [33], [34]. This makes their on-board implementation very expensive since higher computational complexities lead to larger computing delays and increased power consumption. On the other hand, the IDLA and DLA-based polynomial DPD approaches can outperform the pth-order inverse method as suggested in [45]. Furthermore, an exact inverse of a Volterra system is difficult to construct, and the p-th order inverse is only an approximation [3]. Therefore, on the account of computational complexity and power consumption, the LUTs-based, NN-based and p-th order inverse-based DPD methods are usually practical for on-board implementation in narrowband applications only, which is not the scope of HTS. The successive interference cancellation (SIC)-based DPD methods offer sound linearization performance. However, they are also not feasible for HTS as they are typically implemented as data (symbol) predistorters [4], [28]. Data DPD can either be implemented on-ground in gateways, or on-board in regenerative payloads. However, both scenarios are not in the scope of future HTS. In addition, SIC-based DPD methods are non-bandlimited in nature, require a large

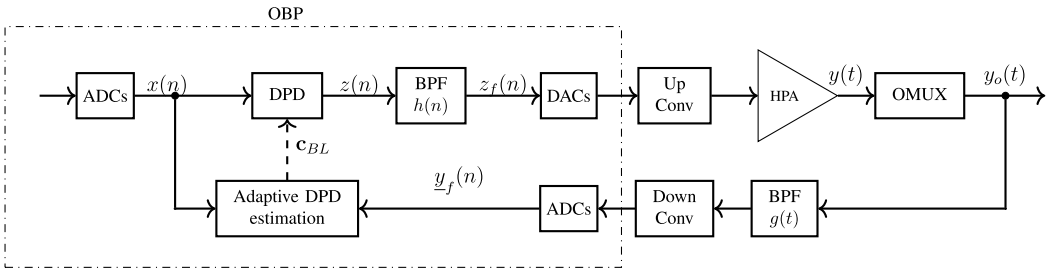

FIGURE 2. Transponder architecture for bandlimited, on-board, adaptive, signal DPD.

number of internal iterations, and their open loop structure is sensitive to loop maladjustments [46]. On the other hand, MPs are extensively used in the literature to implement signal DPD for both in-direct (IDLA) [3], [47] and direct learning architectures (DLA) [22], [25]. The low computational complexity and linear parameterization of MPs makes them well suited for on-board DPD. The IDLA-based DPD approaches exhibit lower computational complexity compared to the DLA-based DPD methods, and are better suited for on-board implementations where the processing power is limited. Therefore, this work focuses on the IDLA-based DPD to perform the system parameter identification analysis.

C. PROPOSED DPD FOR HTS AND THE SYSTEM PARAMETER IDENTIFICATION

This article considers the on-board application of a ground-based DPD, presented in [10], as a practical predistortion approach for HTS. The DPD in [10] was implemented at the gateway, hence referred to as a ground-based DPD. This work extends the DPD in [10] to an on-board implementation. More importantly, the proposed DPD is implemented to perform the system parameter identification analysis to further optimize the predistortion gains. The MP-based DPD in [10] is low-effort and can easily be extended to an on-board application. The considered DPD belongs to the class of signal predistorters. Note that the future HTS will implement transparent architectures with OBPs. As a result, the signal DPD implementations are more feasible when compared to data DPD methods. The on-board data DPD can only be implemented in regenerative payloads. Furthermore, the DPD in [10] is adaptive and bandlimited in nature. Adaptive DPD not only compensates for HPA non-linearities, but also tracks the changes in the uplink-signal characteristics. Furthermore, the bandlimited nature of the considered DPD allows the use of low sampling rate ADCs, DACs and DSPs. The IDLA-based MP DPD method detailed in [10] meets all the criteria for a practical HTS DPD approach, i.e., a **digital, signal, on-board, adaptive** and **bandlimited** implementation with **low complexity**.

Figure 2 presents the transponder architecture considered in this work for the on-board implementation of the ground-based bandlimited MP DPD. Note that in Figure 2, the feedback signal is taken from the output of the OMUX instead of the HPA. This allows the DPD to also mitigate the memory effects of the OMUX. The OMUX filters out the spectral regrowth from the HPA output, therefore it inherently serves as a bandlimiting filter for the HPA output. Moreover, the bandwidth in the feedback path can be further restricted by employing an analog bandpass filter (BPF) $g(t)$ to allow the use of more cheaper and less power consuming ADCs. $h(n)$ is the forward path DPD filter which bandlimits the DPD output. The bandwidth of the BPF $h(n)$ determines the band in which predistortion occurs. It is assumed that the ADC and DAC in Figure 2 have sampling rates equal to atleast twice the passband bandwidth of $g(t)$ and $h(n)$, respectively. The effect of varying the bandwidth of the bandlimiting filters $g(t)$ and $h(n)$ is presented in the simulation results section, and is one of the main contributions of this work. Bandlimited predistortion was initially introduced in terrestrial communication [8], [22], [42], typically implemented at the gateway. However, due to the advent of OBPs, bandlimited DPD approaches are also gaining popularity in on-board applications. Although, the DPD in [10] considers bandlimitation in the forward and feedback path, the DPD performance is analysed only for fixed bandwidths of $g(t)$ and $h(n)$. It is vital to study the effects of varying the bandwidth of the bandlimiting filters $g(t)$ and $h(n)$, as their bandwidth directly influences the required sampling rates for ADCs and DACs (See Figure 2). Table 3 presents the typical bit-resolution, maximum supported sampling rates and power consumption for a few radiation-hardened space grade ADCs. It is clear from Table 3 that the higher sampling rate ADCs are only available for low bit-resolutions. In addition, for higher sampling rates, the ADCs consume more power too. Note that reducing the bandwidth of the bandlimiting filters $g(t)$ and $h(n)$ would lead to a requirement of lower sampling rates for the ADC and DAC in Figure 2. This in turn would lead to a reduced power consumption, and a higher bit-resolution conversion. A higher bit-resolution in converters introduces smaller quantization noise which would increase the overall accuracy of the DPD coefficients estimation process. Therefore, it is important to analyze the effects of changing the bandwidth of $g(t)$ and $h(n)$ on the DPD performance. More importantly, a thorough analysis should be performed to find out how low the bandwidth of these filters can be to still achieve a feasible DPD gain. The next section details the mathematical framework for the IDLA-based bandlimited MP DPD.

TABLE 3. Radiation hardened ADCs.

ADC Type	No. of Bits	Max. Sampling Frequency/MHz	Power Consumption/mW
ADC08D1000/NS	8	1000	1600
STS8388B/AT	8	1000	3400
SPP/AU	12	5	500
AD9042/AD	12	41	545
AD6645/AD	14	105	1500
92040LP/MX	14	10	355
AD977A/AD	16+	0.2	100
7809LP/MX	16+	0.1	132

IV. MATHEMATICAL FRAMEWORK

MPs introduced in Section II are utilized to implement the bandlimited DPD presented in [10]. Using MPs, the DPD output in Figure 2 reads

$$z_f(n) = \sum_{k=1}^{K}\sum_{q=0}^{Q} c_{kq,BL}\left[\sum_{i=0}^{L} x(n-q-i)\,|x(n-q-i)|^{k-1}\,h(i)\right], \quad (4)$$

where $x(n)$ and $z_f(n)$ are the DPD input and output, respectively. K and Q are the non-linearity order and the maximum memory depth of the predistorter, respectively. $c_{kq}\ \forall k = 1\cdots K,\ \forall q = 0\cdots Q$ are the MP DPD model coefficients. Let

$$\hat{x}_{BL}(n,k,q) = \sum_{i=1}^{L} x(n-q)\,|x(n-q)|^{k-1}\,h(i), \quad (5a)$$

$$\hat{\mathbf{x}}_{n,BL} = [\hat{x}(n,1,0)\hat{x}(n,1,1)\cdots\hat{x}(n,K,Q)]^{\mathrm{T}}, \quad (5b)$$

then the MP DPD model in (4) can be written compactly as

$$z_f(n) = \hat{\mathbf{x}}_n^{\mathrm{T}}\mathbf{c}_{BL}. \quad (6a)$$

For a block size of N input samples, i.e., $\mathbf{x} = [x(0)\quad x(1)\quad\cdots\quad x(N-1)]^{\mathrm{T}}$, the MP model for the DPD in matrix form reads

$$\mathbf{z}_f = \hat{\mathbf{X}}_f\mathbf{c}_{BL} \text{ where, } \hat{\mathbf{X}}_f = [\hat{\mathbf{x}}_{0,BL}\quad\hat{\mathbf{x}}_{1,BL}\cdots\hat{\mathbf{x}}_{N-1,BL}]^{\mathrm{T}}, \quad (7)$$

where the entries of the matrix $\hat{\mathbf{X}}_f$ are defined in (5). Assuming the HPA non-linearity is invertible, least squares (LS) can be applied to obtain the DPD coefficients.

$$\mathbf{c}_{BL} = (\hat{\mathbf{Y}}_f^H\hat{\mathbf{Y}}_f)^{-1}\hat{\mathbf{Y}}_f^H\mathbf{z}_f, \quad (8)$$

where $\hat{\mathbf{Y}}_f$ is defined the same way as $\hat{\mathbf{X}}_f$. Note that $\underline{y}_f$ is the actual measured OMUX output in the feedback path. The above described methodology is made iterative for a better training of the predistorter. For the first iteration the DPD coefficients have a trivial solution, i.e., $\mathbf{c} = [1\quad 0\cdots 0]^{\mathrm{T}}$. Table 4 describes the iterative IDLA-based DPD.

TABLE 4. Iterative IDLA-based bandlimited MP DPD.

known parameters: $K, Q, I_{max}, \underline{y}_f$

Initialization $\mathbf{c}_{(0)BL} = 1$,

Iteration $1 \leq i \leq I_{max}$:

$\mathbf{z}_f = \hat{\mathbf{X}}_f\mathbf{c}_{(i-1),BL}$;

$\mathbf{c}_{(i),BL} = (\hat{\underline{\mathbf{Y}}}_f^H\hat{\underline{\mathbf{Y}}}_f)^{-1}\hat{\underline{\mathbf{Y}}}^H\mathbf{z}_f$;

$i = i+1$;

V. SIMULATION RESULTS

This section presents the simulation results of a thorough investigation made to identify the system parameters which effect the performance of the DPD method presented in Section IV. These parameters include the uplink-signal characteristics, the OMUX bandwidth and the operating IBO of the transponder, the order (K) and memory (Q) of the DPD, and the sampling bandwidths of the forward path $h(t)$ and feedback path $g(t)$ filter. In addition, different aspects of DPD are also discussed such as the effect of DPD on power efficiency and unfair DPD gains among the different carriers. The presented results not only highlight the key parameters, but also the scenarios where it makes sense to employ on-board DPD. To the authors best knowledge, no previously reported work provides such an in depth system parameter identification analysis. Furthermore, this section also provides an overview of which of the key performance parameters can be adjusted during the run-time of satellite, and which parameters have to be set during the design phase. In this article different performance metrics are utilized including the bit error rates (BERs), power spectral densities (PSDs), and total degradation (TD) [48]. TD serves as a complete metric to analyze the DPD gain achieved over a given non-linear channel [48]. It is defined as

$$\mathrm{TD[dB]} = \mathrm{OBO[dB]} + \left[\frac{E_s}{N_o}\right]_{req}^{NL}[\mathrm{dB}] - \left[\frac{E_s}{N_o}\right]_{req}^{AWGN}[\mathrm{dB}], \quad (9)$$

where $\left[\frac{E_s}{N_o}\right]_{req}^{NL}$ and $\left[\frac{E_s}{N_o}\right]_{req}^{AWGN}$ represent the symbol energy to noise density ratio required to achieve a target BER for the non-linear and linear (AWGN) channel. OBO is the output back-off, and is defined in Figure 1a.

A. UPLINK-SIGNAL CHARACTERISTICS VS. DPD PERFORMANCE

Uplink-signal characteristics such as the modulation schemes, the forward error correction (FEC) code rates, and the number of carriers affect the DPD gain, and should be tracked adaptively. To study these effects the IDLA-based MP DPD presented in Section IV is implemented without additional bandlimitation in the feedback path. For simulation purposes the "no additional bandlimitation" refers to the case when the bandwidth (BW) of the feedback path filter $g(t)$ is set much larger (2 times or more) than the uplink-signal BW. The normalized non-linear HPA characteristics are defined

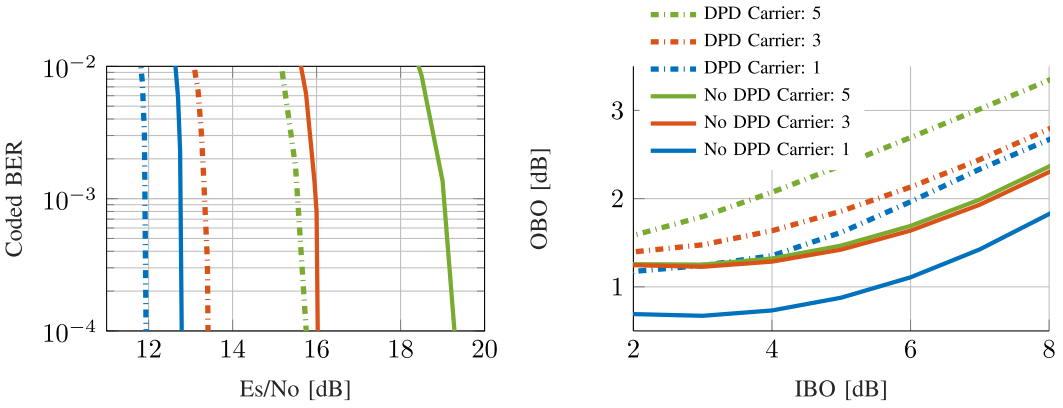

(a) Middle Carrier, IBO 6 dB

(b) Power efficiency

FIGURE 3. Multicarrier operation Vs DPD gain, DPD method: IDLA, Modulation: 16 APSK, Code rate: 5/6, Carriers: 3.

in Figure 1a, given by the Saleh model. The simulated Saleh model coefficients are listed in [16, Table 3, TWT#1]. A 15% OMUX guard band is utilized, i.e., the OMUX 3 dB BW is 15% more than the uplink-signal BW. The fixed-point-arithmetic (FPA) design of the digital components and quantization effects of the ADCs/DACs have not been considered in the presented results, and is left as a future work. Unless stated otherwise, the bandwidth of the forward path DPD filter $h(n)$ is set to 1.5 times the uplink-signal BW, and all the carriers have equal power and symbol rates. It should be noted that although the HPA is modeled using the memoryless Saleh model, the transponder still exhibits memory due to the presence of the IMUX and OMUX. The simulations are performed in Matlab where each block in Figure 2 is modelled as an object oriented block. Similar programming framework is employed in [10], [19].

1) NUMBER OF CARRIERS VS. DPD GAIN

The multicarrier operation of the transponder increases the bandwidth efficiency, but it also effects the DPD performance as depicted in Figure 3a. The BER curve labels and OBOs for each scenario are plotted in Figure 3b. It can be observed from Figure 3a that when a multicarrier signal is uplinked to the HTS, the gain in BER performance is higher. This is because the multicarrier signals introduce IMD and ICI, leading to severe clustering and warping effects. Moreover, the higher the number of carriers within the transponder BW, the more significant these effects are, and the more DPD has to compensate for. In addition, the multicarrier operation also affects the power efficiency of the HTS transponder. A multicarrier operation generates IMD products, and the HPA output power is shared between the useful carriers and the IMD noise [7] which influences the overall power efficiency. This is clear from Figure 3b, where the multicarrier signals exhibit higher OBOs for each IBO, thus reducing the power efficiency.

2) MODULATION AND CODING RATES VS. DPD GAIN

Modulation and coding rates (ModCods) also affect the DPD gain as depicted in Figure 4a and Figure 4b, respectively. The BER curves are plotted for an IBO of 6 dB, and the respective OBO for each scenario can be estimated from Figure 4c and Figure 4d. It can be seen from Figure 4a and Figure 4b that when a higher modulation order and a larger code rate is employed, the gain in BER performance is more significant, i.e., a higher DPD gain. The non-linear effects are higher at higher ModCods [9], as a result, the DPD has more to compensate for, thus leading to a much larger gain. Furthermore, it is clear from Figure 4c and Figure 4d that the OBO is influenced by the changes in modulation order but not the code rate. It should be noted that DPD leads to a rise in OBO (see Figure 4c and Figure 4d), but it also reduces the SNR ($\frac{Es}{No}$) required to achieve a certain target BER. Therefore, for an over all gain in performance, DPD should only be considered for those scenarios or parameters where the rise in OBO is smaller than the gain in BER performance. Under these conditions, DPD would lead to an overall reduction in TD. From Figure 3 and Figure 4, it is clear that DPD should be considered for higher ModCods and multicarrier uplink signals. A multicarrier transmission leads to higher a bandwidth efficiency, and the higher ModCods increase the throughput. Moreover note that the varying DPD gains due to the changing uplink-signal characteristics confirms the need for adaptive DPD.

B. TRANSPONDER PARAMETERS VS. DPD GAIN

Transponder characteristics such as the transponder BW (OMUX BW) and the HPA's operating point also affect the DPD performance. These effects are discussed in the following. The OMUX BW has an impact on the BER performance [4]. Figure 5a presents the BER performance for two different OMUX bandwidths, i.e., with a guardband of 15% and 20%. From Figure 5a, it is clear that the smaller OMUX BW (15% more than signal BW) introduces more severe distortions in

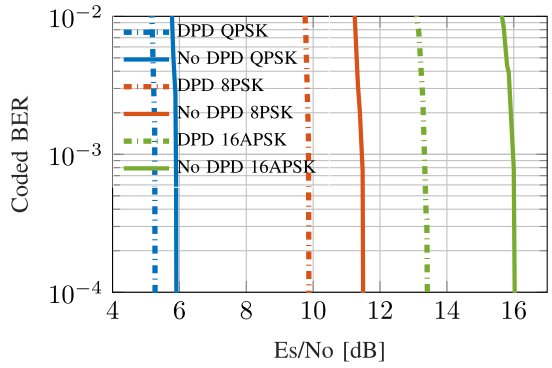

(a) Modulation Vs. DPD gain, **Middle carrier**, Code rate (CR): 5/6, IBO: 6 dB

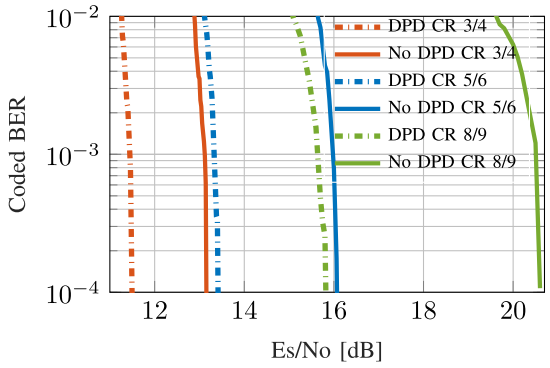

(b) Code rate Vs. DPD gain, **Middle carrier**, Mod: 16APSK, IBO: 6 dB

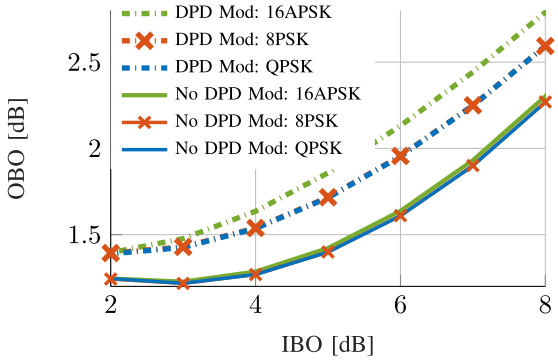

(c) Modulation Vs. Power efficiency, Code rate (CR): 5/6

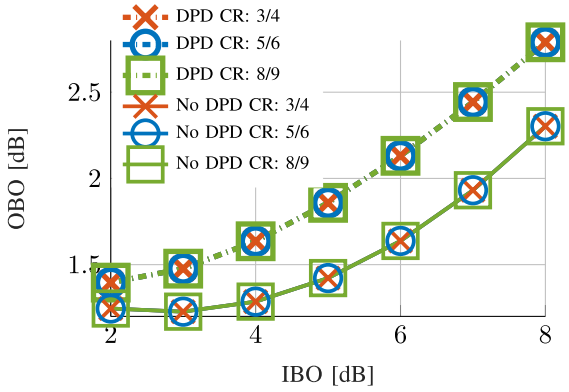

(d) Code rate Vs. Power efficiency, Mod: 16APSK

FIGURE 4. **ModCods vs DPD gain and power efficiency (OBO), DPD method: IDLA, Carriers: 3.**

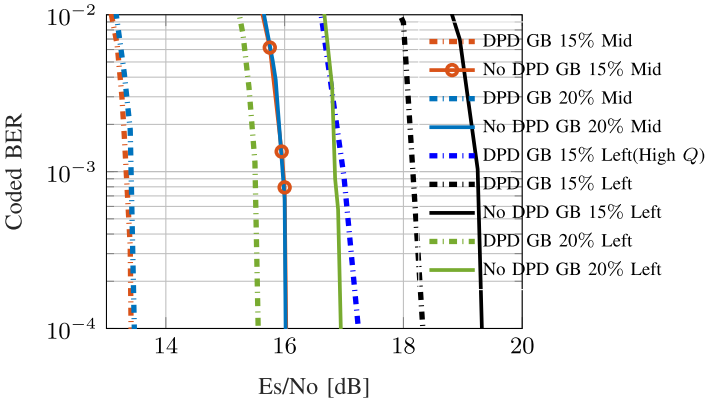

(a) OMUX guard band (GB) Vs. DPD gain

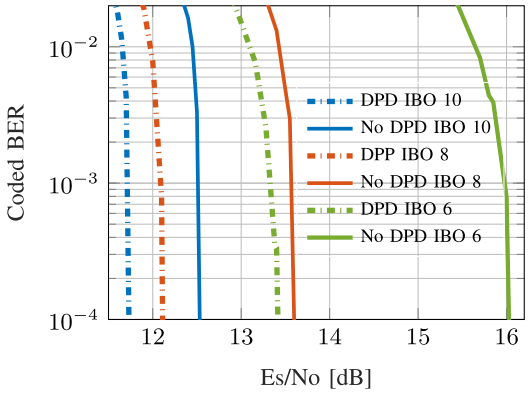

(b) Operating point Vs. DPD gain

FIGURE 5. **Transponder parameters Vs DPD gain, DPD method: IDLA, Modulation: 16 APSK, Code rate: 5/6, Carriers: 3.**

the downlink signal, especially in the edge carriers, while the middle carriers remain more or less un-affected by the variable OMUX BW. This is because the group delay profile of the OMUX varies extremely at the edges, while it is flat in the middle. Nonetheless, DPD provides a gain for both the middle and the edge carrier. Note that for a tighter OMUX BW, a higher DPD memory (Q) is needed to achieve a comparable gain to a relaxed (wider) OMUX BW scenario. The effects of memory on DPD performance will be discussed in more detail in the following sections. In addition, it is also clear from Figure 5b that DPD leads to a higher gain in BER performance for an HPA operation closer to saturation, i.e., a lower IBO. This is because a lower IBO operation introduces more severe non-linearities in the amplified signal. As a result, there is more for the DPD to compensate for. Thus employing DPD, especially closer to saturation not only provides a larger BER gain but also increases the power efficiency. From Figure 5, it is clear that when implementing

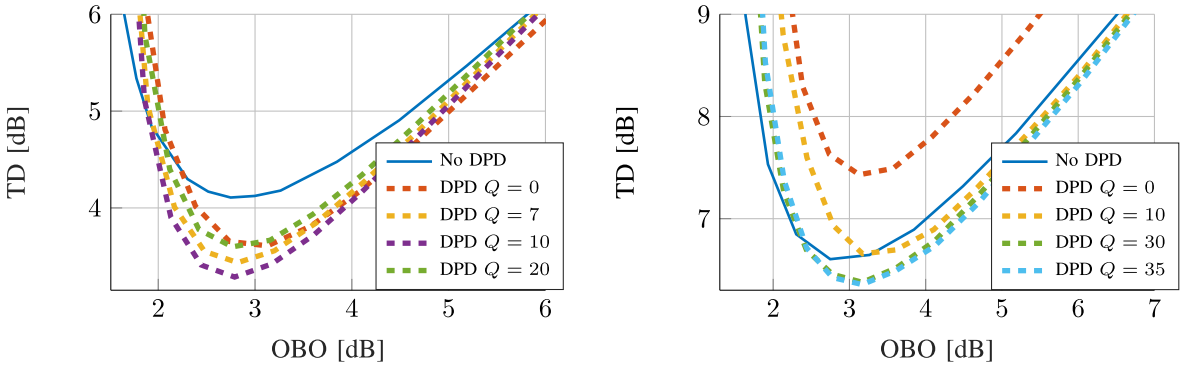

(a) Middle Carrier

(b) Edge (left) Carrier

FIGURE 6. Effect of memory on DPD performance, DPD method: IDLA, $K = 3$.

DPD, the OMUX BW and the operating point should be kept in mind among the key parameters affecting the DPD performance.

C. PREDISTORTION ALGORITHM PARAMETERS VS. DPD GAIN

This section analyzes the DPD performance for varying the predistortion algorithm specific parameters. For the implemented DPD, this involves the memory and order. In addition, the carrier fairness aspects of DPD are also discussed here. Furthermore, a power consumption analysis for the proposed DPD is also provided. For this and the coming subsections, unless stated otherwise, a 3 carrier 16-APSK modulated signal with an FEC code rate of 5/6 is uplinked to the satellite. In addition, all the carriers have equal power and symbol rates. The OMUX guardband is 15% and no additional bandlimitation is considered. The forward path DPD filter $h(n)$ bandwidth is set to 1.5 times the uplink-signal BW.

1) MEMORY (Q) VS. DPD GAIN

DPD with appropriate modeling can compensate for memory effects introduced by the transponder filters and the HPA. Figure 6 presents the TD performance of the considered IDLA-based DPD for different memory depths. It can be observed from Figure 6a that when the memory (Q) is increased from 0 to 10 there is a reduction in TD and the optimal OBO for the middle carrier. However, if the memory depth (Q) is increased significantly (e.g., $Q = 20$), the TD rises, i.e., DPD performance suffers. This could be due to the fact that at higher memory depths, the larger size of the matrix to be inverted can create numerical problems, leading to in-accurate inversions in (8). For a typical OMUX, the carriers in the middle are least affected by the memory effects, hence large memory depths of DPD are not required. Even a memory $Q = 0$ provides a reduction in TD for the middle carrier. However, the edge carriers suffer from more severe memory effects, hence DPD with $Q = 0$ leads to a poor performance as depicted in Figure 6b. A reduction in TD is also observed for the edge carrier when the memory is increased. In addition, increasing the memory eventually saturates the DPD performance (See Figure 6b). This is because increasing the DPD memory beyond a certain point would only lead to minimal or no gain as all the memory effects introduced by the HPA and the transponder filters would have already been compensated for. Also note that the reduction in TD is more significant for the middle carrier when compared to the edge carrier. This is because the middle carrier suffers from more severe non-linear effects such as ICI or IMD noise which can be greatly reduced when DPD is implemented. Note that the memory also influences the computational load on the OBP. A higher memory of DPD implies larger matrix inversions which requires more computational power, and can lead to computing delays.

2) ORDER (K) VS. DPD GAIN

The order of the DPD is another parameter which influences the DPD performance. Typically, for stronger HPA non-linearities, a higher order (K) of the DPD is required. Figure 7 presents the TD performance of the IDLA-based DPD for different orders (K). Figure 7 exhibits a slight gain in performance when the order of the DPD is increased from 3 to 5, indicating that some 5^{th} order non-linearities are present in the system. Moreover, the performance suffers in terms of power efficiency when the order is increased to 7 (a higher optimal IBO, see Figure 7a). This could be attributed to the fact that the larger size of the matrix to be inverted can create numerical problems, leading to in-accurate inversions in (8). However for the current simulation setup, it is clear that the order $K = 3$ for the DPD is sufficient. Also, a lower order reduces the computational complexity of the DPD which is an added benefit, especially in on-board DPD applications where the computational power is limited. It is clear from Figure 6 and Figure 7 that the memory of the predistorter plays a more vital role in the DPD performance when compared to the order of the predistorter. Nonetheless, both parameters should be kept in mind when implementing and optimizing DPD performance, especially when the processing power is limited.

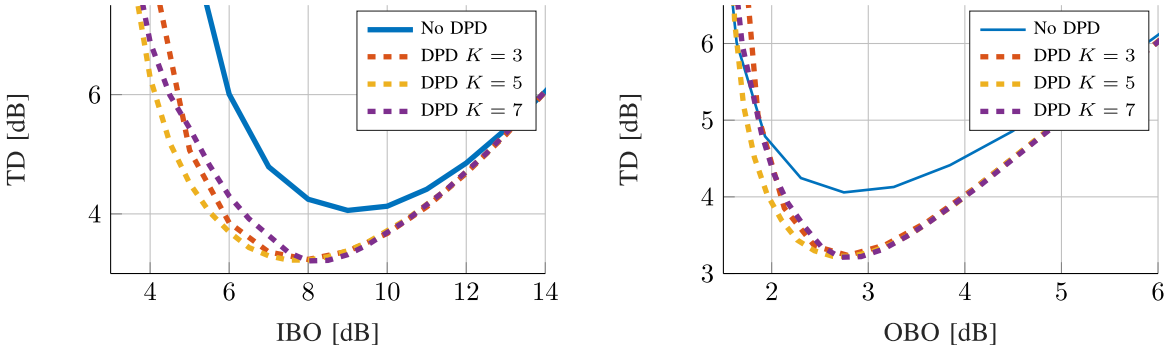

(a) Middle carrier: IBO Vs TD (b) Middle carrier: OBO Vs TD

FIGURE 7. Effect of Order on DPD performance, DPD method: IDLA, $Q = 10$.

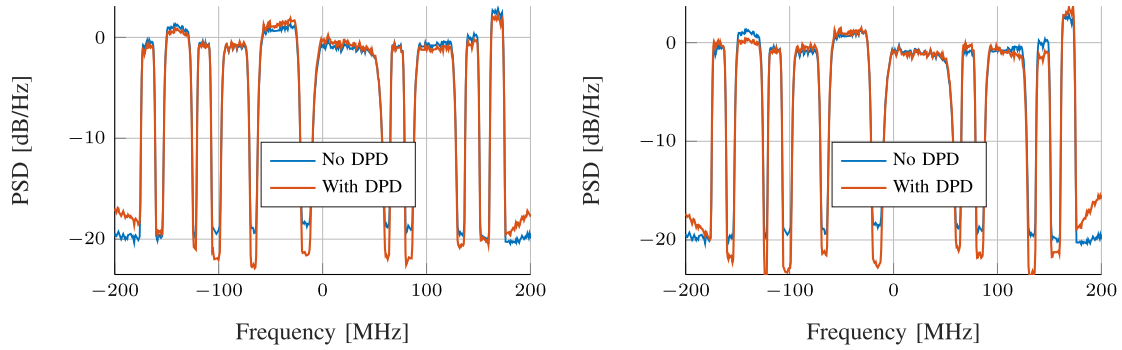

(a) Memory ($Q = 5$) (b) Memory ($Q = 10$)

FIGURE 8. DPD gain for different carriers. DPD Method: IDLA, $K = 3$, IBO: 8 dB.

It should be noted that the computational complexity directly translates to the power consumed. The running computational complexity of the MP-based DPD is presented in [49, Table 1]. The power consumed per sample by the MP-based DPD in the forward path is also calculated in [49], and is given below.

$$P_{\text{DPD}} = E_{\text{cycle}}\left(\frac{7}{2} \cdot K \cdot Q + \frac{9}{2}\right), \tag{10}$$

where E_{cycle} is the energy consumption per cycle of a fixed-point digital signal processor (DSP). For $K = 3$, $Q = 10$, $N = 64800$, and $E_{\text{cycle}} = 150\frac{\text{pWs}}{\text{cycle}}$, the power consumed by the DPD in the forward path is 1.1 mW. It is to be noted that in these calculations, the effect of the word-lengths as well as data storage and communication are not included as they are highly dependent on the chosen hardware and architecture. Note that (10) only presents the power consumed by the DPD in the forward path. The power consumed by the DPD in the feedback path depends on the identification complexity. Identification of the DPD coefficients requires an inverse (See (8)). Estimating the power consumed in the identification process is not trivial as it is dependent on how the inverse is computed. This task has been left by the authors as a future work.

3) DPD AND CARRIER FAIRNESS ASPECTS

In certain scenarios DPD can be unfair. Here unfairness implies that DPD may prefer some carriers over the others, even though the same DPD coefficients are applied to all the carriers. Figure 8 demonstrates the carrier fairness aspect of DPD, when applied to a 10-carrier signal. The simulated carriers have unequal power and bandwidths. Figure 8 presents the normalized PSD of the received signal. Note that a higher peak of the PSD, and a lower IMD noise implies a larger received carrier to noise ratio (CNR). A higher CNR would lead to a lower BER. From Figure 8, it is clear that the gain in CNR is different for each carrier when DPD is applied. Especially the powerful carriers are favored, while the carriers nearby the powerful carriers or at the edges are disadvantaged, and they may exhibit a smaller or a reduced CNR gain. Moreover, the PSD performance changes when a different memory depth is considered as depicted in Figure 8a and Figure 8b. Therefore, in scenarios with different carrier powers and bandwidths, the carrier fairness aspect should be kept in mind.

D. BANDLIMITATION VS. DPD GAIN

Sections V-A to V-C presented the uplink-signal, transponder and DPD parameters which affect the predistortion gain. The results were presented for "no additional bandlimitation" case. This section covers the effect of additional bandlimitation on the DPD performance. More importantly, this section investigates on how low the feedback path filter $g(t)$ and forward path DPD filter $h(n)$ bandwidths can be to still achieve a gain when DPD is implemented.

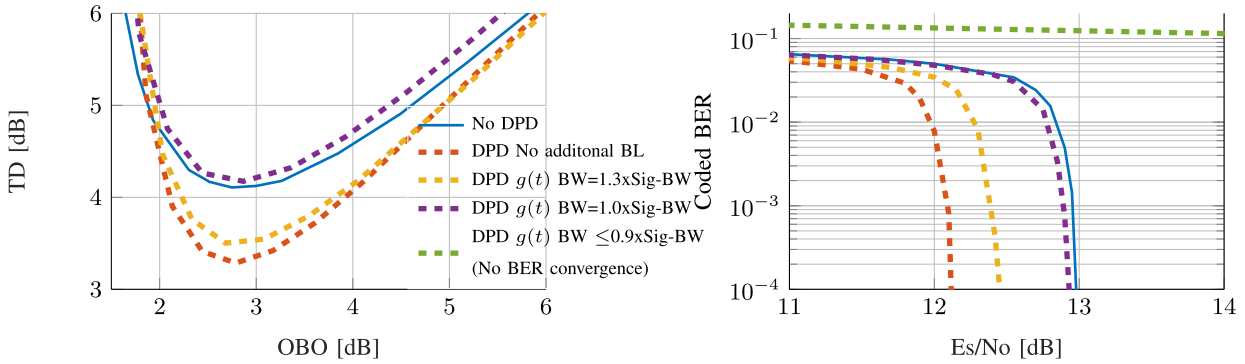

(a) Middle carrier: OBO Vs TD

(b) Middle carrier: BER performance

FIGURE 9. Bandlimitation in the feedback path. DPD Method: IDLA, $K = 3$, $Q = 10$.

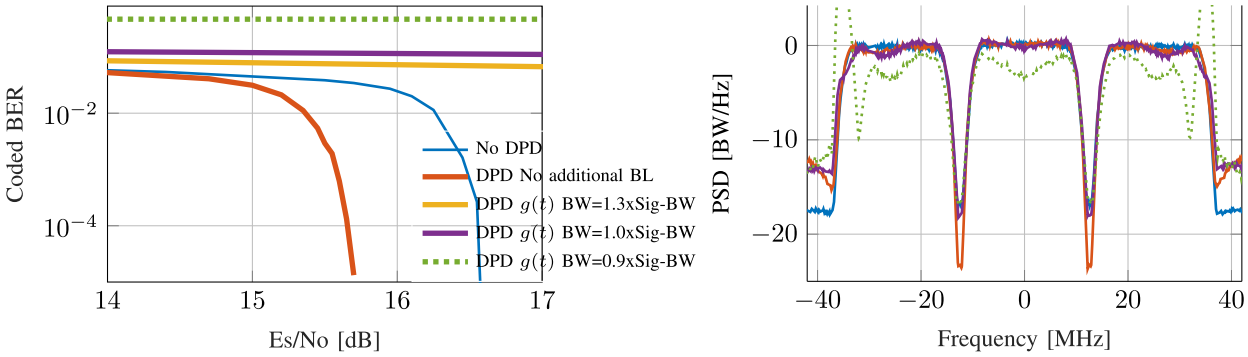

(a) Edge carrier: BER Performance

(b) PSD performance

FIGURE 10. Bandlimitation in the feedback path. DPD Method: IDLA, $K = 3$, $Q = 10$, OBO w/o DPD: 2.3 dB, OBO with DPD: 2.7 dB.

1) BANDLIMITATION FEEDBACK PATH

Bandlimitation in the feedback path is introduced via the analog bandpass filter $g(t)$ (See Figure 2). The bandlimitation helps reduce the burden on the sampling and processing rates of the ADCs and DSPs involved in the estimation of the DPD coefficients. Figure 9 presents the effect of bandlimitation on the performance of the considered MP-based bandlimited DPD in terms of TD and BER for the middle carrier. It is observed that when the bandwidth of the analog bandpass filter $g(t)$ is reduced, the DPD performance suffers. This is because the vital HPA output information needed to estimate the optimal DPD coefficients gets cut due to the bandlimitation. Moreover, since the filter $g(t)$ is an analog bandpass filter, it also exhibits non-ideal filter characteristics. As a result, $g(t)$ not only cuts the feedback signal but also adds linear and non-linear distortions to it. This also effects the estimation of the DPD coefficients. Note that the best performance for the middle carrier is observed for the curve labeled "No additional BL" which inherently includes the bandlimitation from the OMUX. Figure 10a presents the effect of bandlimitation on the BER performance for the edge carrier. It is observed that performing additional bandlimitation leads to a much severe loss in BER performance for the edge carrier compared to the middle carrier. This is because the feedback filter $g(t)$ adds more severe linear and non-linear distortions to the edge carrier. Figure 10b presents the PSD at the HPA output for the bandlimitation scenario presented in Figure 9 and Figure 10a. The PSD results are consistent with the provided TD and BER results. From Figure 10b, it is observed that when no additional bandlimitation is considered, the HPA output signal exhibits the least IMD noise, leading to the best performance. Note that when the feedback BW is limited to the signal BW, the IMD noise and ACPRs rise. In addition, the HPA output is distorted for the edge carriers, hence no BER convergence (see Figure 10a). Furthermore, when the bandwidth of $g(t)$ is reduced below the signal BW (e.g., 0.9xSig-BW), the HPA output is completely distorted for all the carriers, making it impossible to recover the transmitted data. Therefore, when the presented IDLA-based MP DPD is implemented, "no additional bandlimitation" should be considered.

2) BANDLIMITATION FORWARD PATH

Bandlimitation in the forward path is introduced by a digital bandpass filter $h(n)$ to allow the use of low speed DACs in the OBPs. The filter $h(n)$ determines the band in which the DPD occurs. As a result, the bandwidth of $h(n)$ cannot be reduced below the signal BW, as this would cut the signal itself in the forward path before amplification. Figure 11

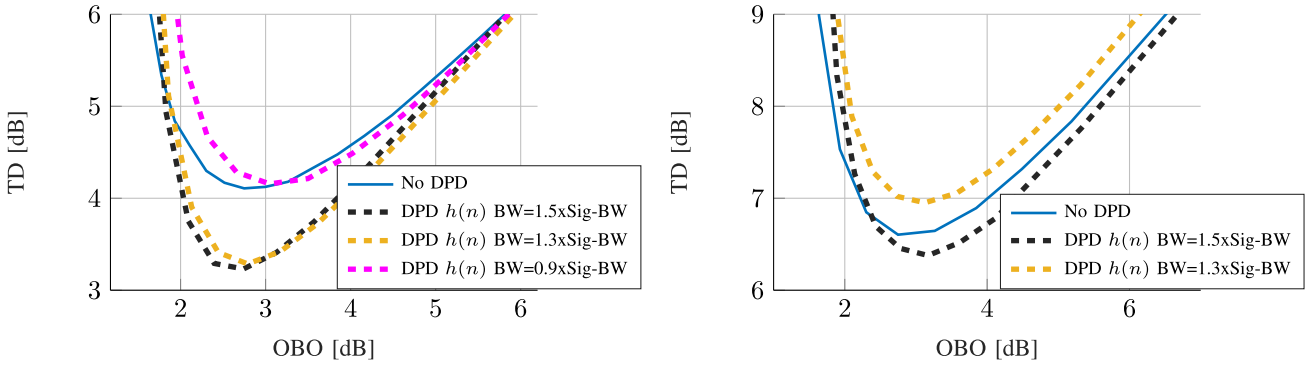

(a) Middle carrier, DPD method: IDLA: $K = 3$ $Q = 10$

(b) Edge carrier, DPD method: IDLA: $K = 3$ $Q = 30$

FIGURE 11. Bandlimitation in the forward path, No additional bandlimitation in feedback path.

presents the effect of reducing the bandwidth of $h(n)$ on the performance of the proposed DPD method in terms of TD. For the simulated scenario, in the case of the middle carrier, the TD performance remains more or less the same when the bandwidth of $h(n)$ is reduced from 1.5 to 1.3 times the uplink-signal BW (See Figure 11a). However, the same reduction in bandwidth severely effects the edge carrier TD performance as depicted in Figure 11b. This is because $h(n)$ is a non-ideal bandpass filter, and a tighter $h(n)$ adds more severe linear and non-linear distortions to the input, especially to the edge carriers. Nonetheless, for the given scenario a bandwidth of 1.5xSignal-BW is needed for implementing the proposed DPD method. It is clear from the presented bandlimitation analysis that the bandwidth of the feedback path $g(t)$ and forward path $h(n)$ filter plays a key role in determining the DPD performance. As a result, the two parameters should be kept in mind when designing and implementing bandlimited DPD.

E. PARAMETER ADJUSTMENT AND DESIGN

For a better understanding of the application of DPD in satellite payloads, it is equally important to understand where the identified parameters can be set or changed. The key performance parameters can be either adjusted during the normal operation of the satellite, or they have to be set optimally during the payload design phase. To cope with the data traffic demand, the uplink-signal parameters such as the ModCods and number of carriers are often changed during the run-time of the satellite. The adaptive DPD can track the changes in the uplink-signal characteristics, and perform predistortion optimally. In addition, the parameters like the bandwidth of the forward-path bandlimiting filter $h(n)$, memory (Q) and order (K) of the DPD, HPA's operating point (IBO), and sampling rates of ADCs/DACs can be adjusted during the normal satellite operation. A quick offline analysis can be performed for these parameters, for example during the service or downtime of the satellite. Once an optimal performance is achieved, the parameters can be adjusted on-board the satellite using the control commands from the ground station. On the other hand, parameters like the bandwidth of the OMUX and the feedback path filter $g(t)$ have to be set during the design phase of the transponder, i.e., pre-launch. Furthermore, the bit-resolution of the converters is also set during the design phase. However, the upcoming digital payload designs also offer reconfigurable ADCs, DACs, and FPGAs [50].

VI. CONCLUSION

The paper presented the results of a thorough investigation made to identify the critical system parameters which affect the predistortion performance. The studied parameters included the uplink-signal, transponder and predistortion algorithm specific parameters. For the presented analysis, a ground-based state-of-the-art bandlimited MP DPD was implemented in an on-board application. The presented parameter identification analysis highlighted the scenarios where DPD implementation led to the maximum DPD gain such as multicarrier uplink signals with higher ModCods, an operation closer to saturation, and transponders with tighter OMUX bandwidths. Furthermore, the effect of changing the memory and order of the DPD was discussed in detail. It was observed that memory played a more critical role in the DPD performance, and should be set optimally. Otherwise, an overcompensation of the memory may not only lead to a higher computational complexity, but a reduction in performance due to the increased numerical instability issues. More importantly, the paper also analyzed the effect of bandlimitation on the performance of the state-of-the-art DPD method. It was found out that while implementing the considered state-of-the-art DPD, the bandwidth in the critical feedback path cannot be reduced below the uplink signal bandwidth. The analysis also revealed that adaptive linearization is vital for future HTS.

The paper also provided a general insight into the on-board signal processing capabilities of HTS, especially in terms of the available processing power and the sampling rates. Even though the signal processing capabilities have significantly improved lately, they are still limited on-board the satellite. Therefore, it is vital to process the most relevant data and

only involve the operations which lead to the desired result. The presented system parameter identification analysis provided an insight into which parameters and trade-offs are the most beneficial in terms of predistortion, provided sufficient resources are available to implement a complete on-board predistortion solution.

REFERENCES

[1] "5G: Challenges, research priorities, and recommendations," A. Joint Consortium 5G-PPP, Berlin, Germany, Tech. Rep. 2911522, Sep. 2014. [Online]. Available: https://cordis.europa.eu/docs/projects/cnect/5/317105/080/deliverables/001-D15Annex15GChallengesResearchprioritiesandRecommendations.pdf

[2] P. Angeletti, R. De Gaudenzi, and M. Lisi, "From 'bent pipes' to 'software defined payloads': Evolution and trends of satellite communications systems," in *Proc. 26th Int. Commun. Satell. Syst. Conf. (ICSSC)*, 2008, pp. 1–10.

[3] L. Ding, G. T. Zhou, D. R. Morgan, Z. Ma, J. S. Kenney, J. Kim, and C. R. Giardina, "A robust digital baseband predistorter constructed using memory polynomials," *IEEE Trans. Commun.*, vol. 52, no. 1, pp. 159–165, Jan. 2004.

[4] S. Dimitrov, "Non-linear distortion cancellation and symbol-based equalization in satellite forward links," *IEEE Trans. Wireless Commun.*, vol. 16, no. 7, pp. 4489–4502, Jul. 2017.

[5] C. Cripps, *RF Power Amplifers for Wireless Communications*. Norwood, MA, USA: Artech House, 1999.

[6] S. Pupolin and L. Greenstein, "Performance analysis of digital radio links with nonlinear transmit amplifiers," *IEEE J. Sel. Areas Commun.*, vol. 5, no. 3, pp. 534–546, Apr. 1987.

[7] G. E. Corazza, *Digital Satellite Communication*. Boston, MA, USA: Springer, 2007.

[8] C. Yu, L. Guan, and A. Zhu, "Band-limited Volterra series-based behavioral modeling of RF power amplifiers," in *IEEE MTT-S Int. Microw. Symp. Dig.*, Jun. 2012, pp. 1–3.

[9] S. Lim and C. Eun, "Predistorter design for a memory-less nonlinear high power amplifier using the pth-order inverse method for OFDM systems," in *Proc. Int. Symp. Intell. Signal Process. Commun. Syst.*, Dec. 2005, pp. 217–220.

[10] N. Kelly, M. Allegue-Martínez, P.-D. Arapoglou, and A. Zhu, "Bandwidth-constrained digital pre-compensation technique for multi-carrier satellite communications," *Int. J. Satell. Commun. Netw.*, vol. 34, no. 2, pp. 171–194, Mar. 2016.

[11] ETSI EN 302 307-2, "Digital video broadcasting (DVB); second generation framing structure, channel coding and modulation systems for broadcasting, interactive services, news gathering and other broadband satellite applications. technical report part II: S2-extensions (DVB-S2X)," Eur. Telecommun. Standards Inst., Sophia Antipolis, France, Tech. Rep. V1.1.1, 2014.

[12] ETSI EN 302 307-2, "Digital video broadcasting (DVB); implementation guidelines for the second generation system for broadcasting, interactive services, news gathering and other broadband satellite applications; part 2: S2 extensions (DVB-S2X)," Eur. Telecommun. Standards Inst., New Delhi, India, Tech. Rep. A171-2, 2015.

[13] B. F. Beidas, H. El Gamal, and S. Kay, "Iterative interference cancellation for high spectral efficiency satellite communications," *IEEE Trans. Commun.*, vol. 50, no. 1, pp. 31–36, Jan. 2002.

[14] B. F. Beidas, "Intermodulation distortion in multicarrier satellite systems: Analysis and turbo Volterra equalization," *IEEE Trans. Commun.*, vol. 59, no. 6, pp. 1580–1590, Jun. 2011.

[15] G. Maral and M. Bousquet, *Satellite Communications Systems : Systems, Techniques and Technology*, 5th ed. Hoboken, NJ, USA: Wiley, 2014.

[16] A. A. M. Saleh, "Intermodulation analysis of FDMA satellite systems employing compensated and uncompensated TWT's," *IEEE Trans. Commun.*, vol. 30, no. 5, pp. 1233–1242, May 1982.

[17] M. Aloisio, E. Casini, and A. Ginesi, "Evolution of space traveling-wave tube amplifier requirements and specifications for modern communication satellites," *IEEE Trans. Electron Devices*, vol. 54, no. 7, pp. 1587–1596, Jul. 2007.

[18] D. Zhou and V. E. DeBrunner, "Novel adaptive nonlinear predistorters based on the direct learning algorithm," *IEEE Trans. Signal Process.*, vol. 55, no. 1, pp. 120–133, Jan. 2007.

[19] O. B. Usman, G. Staude, and A. Knopp, "Onboard compensation of linear and non-linear hardware imperfections in multiport amplifiers," in *Proc. IEEE Global Commun. Conf. (GLOBECOM)*, Dec. 2018, pp. 1–6.

[20] Xilinx. (2015). *Radiation-Hardened, Space-Grade Virtex-5QV Family Data Sheet: Overview*. [Online]. Available: https://www.xilinx.com/support/documentation/data_sheets/ds192_V5QV_Device_Overview.pdf

[21] XilinX. (2020). *7 Series FPGAs Data Sheet: Overview*. [Online]. Available: https://www.xilinx.com/support/documentation/data_sheets/ds180_7Series_Overview.pdf

[22] Y. Liu, W. Pan, S. Shao, and Y. Tang, "A general digital predistortion architecture using constrained feedback bandwidth for wideband power amplifiers," *IEEE Trans. Microw. Theory Techn.*, vol. 63, no. 5, pp. 1544–1555, May 2015.

[23] J. Liu and V. Mukundagiri, "Study of ADC resolution and bandwidth requirement tradeoffs for high-speed data communications," in *Proc. IEEE 56th Int. Midwest Symp. Circuits Syst. (MWSCAS)*, Aug. 2013, pp. 864–867.

[24] D. R. Morgan, Z. Ma, J. Kim, M. G. Zierdt, and J. Pastalan, "A generalized memory polynomial model for digital predistortion of RF power amplifiers," *IEEE Trans. Signal Process.*, vol. 54, no. 10, pp. 3852–3860, Oct. 2006.

[25] Y. Liu, J. J. Yan, H.-T. Dabag, and P. M. Asbeck, "Novel technique for wideband digital predistortion of power amplifiers with an undersampling ADC," *IEEE Trans. Microw. Theory Techn.*, vol. 62, no. 11, pp. 2604–2617, Nov. 2014.

[26] O. B. Usman, G. Staude, and A. Knopp, "Adaptive onboard compensation of non-linear HPAs and imperfect butler matrices in multiport amplifiers for high throughput satellites," in *Proc. 36th Int. Satell. Commun. Syst. Conf. (ICSSC)*, Oct. 2018, pp. 1–8.

[27] G. Karam and H. Sari, "Data predistortion techniques using intersymbol interpolation," *IEEE Trans. Commun.*, vol. 38, no. 10, pp. 1716–1723, Oct. 1990.

[28] B. F. Beidas, R. I. Seshadri, and N. Becker, "Multicarrier successive predistortion for nonlinear satellite systems," *IEEE Trans. Commun.*, vol. 63, no. 4, pp. 1373–1382, Apr. 2015.

[29] G. Karam and H. Sari, "A data predistortion technique with memory for QAM radio systems," *IEEE Trans. Commun.*, vol. 39, no. 2, pp. 336–344, Feb. 1991.

[30] A. Molina, K. Rajamani, and K. Azadet, "Digital predistortion using lookup tables with linear interpolation and extrapolation: Direct least squares coefficient adaptation," *IEEE Trans. Microw. Theory Techn.*, vol. 65, no. 3, pp. 980–987, Mar. 2017.

[31] N. Naskas and Y. Papananos, "Neural-network-based adaptive baseband predistortion method for RF power amplifiers," *IEEE Trans. Circuits Syst. II, Exp. Briefs*, vol. 51, no. 11, pp. 619–623, Nov. 2004.

[32] M. Rawat, K. Rawat, and F. M. Ghannouchi, "Adaptive digital predistortion of wireless power amplifiers/transmitters using dynamic real-valued focused time-delay line neural networks," *IEEE Trans. Microw. Theory Techn.*, vol. 58, no. 1, pp. 95–104, Jan. 2010.

[33] R. Hongyo, Y. Egashira, T. M. Hone, and K. Yamaguchi, "Deep neural network-based digital predistorter for Doherty power amplifiers," *IEEE Microw. Wireless Compon. Lett.*, vol. 29, no. 2, pp. 146–148, Feb. 2019.

[34] M. Schetzen, "Theory of pth-order inverses of nonlinear systems," *IEEE Trans. Circuits Syst.*, vol. 23, no. 5, pp. 285–291, May 1976.

[35] E. Biglieri, S. Barberis, and M. Catena, "Analysis and compensation of nonlinearities in digital transmission systems," *IEEE J. Sel. Areas Commun.*, vol. SAC-6, no. 1, pp. 42–51, Jan. 1988.

[36] A. A. M. Saleh, "Frequency-independent and frequency-dependent nonlinear models of TWT amplifiers," *IEEE Trans. Commun.*, vol. 29, no. 11, pp. 1715–1720, Nov. 1981.

[37] E. Costa, M. Midrio, and S. Pupolin, "Impact of amplifier nonlinearities on OFDM transmission system performance," *IEEE Commun. Lett.*, vol. 3, no. 2, pp. 37–39, Feb. 1999.

[38] E. Aschbacher and M. Rupp, "Modelling and identification of a nonlinear power-amplifier with memory for nonlinear digital adaptive predistortion," in *Proc. 4th IEEE Workshop Signal Process. Adv. Wireless Commun. (SPAWC)*, Jun. 2003, pp. 658–662.

[39] C. Rapp, "Effects of HPA-nonlinearity on 4-DPSK/OFDM-signal for a digital sound broadcasting system," *ESA Special Publication*, vol. 332, pp. 179–184, Oct. 1991.

[40] A. Ghorbani and M. Sheikhan, "The effect of solid state power amplifiers (SSPAs) nonlinearities on MPSK and M-QAM signal transmission," in *Proc. 6th Int. Conf. Digit. Process. Signals Commun.*, Sep. 1991, pp. 193–197.

[41] A. Zhu, J. C. Pedro, and T. J. Brazil, "Dynamic deviation reduction-based volterra behavioral modeling of RF power amplifiers," *IEEE Trans. Microw. Theory Techn.*, vol. 54, no. 12, pp. 4323–4332, Dec. 2006.
[42] G. Su, W. Chen, S. Zhang, and F. M. Ghannouchi, "A robust and low sampling rate digital predistortion algorithm for broadband PA modeling and predistortion," in *Proc. WAMICON*, Jun. 2014, pp. 1–4.
[43] X. YU, "Contributions to digital predistortion of radio-frequency power amplifiers for wireless applications," Ph.D. dissertation, Dept. Elect. Eng.-Electron.-Inf. Technol. (EEI), Univ. Erlangen-Nürnberg, Erlangen, Germany, 2012.
[44] A. Katz, J. Wood, and D. Chokola, "The evolution of PA linearization: From classic feedforward and feedback through analog and digital predistortion," *IEEE Microw. Mag.*, vol. 17, no. 2, pp. 32–40, Feb. 2016.
[45] B. F. Beidas, "Adaptive digital signal predistortion for nonlinear communication systems using successive methods," *IEEE Trans. Commun.*, vol. 64, no. 5, pp. 2166–2175, May 2016.
[46] M. O'Droma, E. Bertran, M. Gadringer, S. Donati, A. Zhu, P. L. Gilabert, and J. Portilla, "Developments in predistortion and feedforward adaptive power amplifier linearisers," in *Proc. Eur. Gallium Arsenide Other Semiconductor Appl. Symp.*, Oct. 2005, pp. 337–340.
[47] C. Eun and E. J. Powers, "A new Volterra predistorter based on the indirect learning architecture," *IEEE Trans. Signal Process.*, vol. 45, no. 1, pp. 223–227, Jan. 1997.
[48] E. Casini, R. D. Gaudenzi, and A. Ginesi, "DVB-S2 modem algorithms design and performance over typical satellite channels," *Int. J. Satell. Commun. Netw.*, vol. 22, no. 3, pp. 281–318, May 2004, doi: 10.1002/sat.791.
[49] S. Boumard, M. Lasanen, O. Apilo, A. Hekkala, C. Cassan, J.-P. Verdeil, J. David, and L. Pichon, "Power consumption trade-off between power amplifier OBO, DPD, and clipping and filtering," in *Proc. 26th Int. Teletraffic Congr. (ITC)*, Sep. 2014, pp. 1–5.
[50] Xilinx. (2020). *Radiation Tolerant Kintex Ultrascale XQRKU060 FPGA Data Sheet*. [Online]. Available: https://www.xilinx.com/support/documentation/data_sheets/ds882-xqr-kintex-ultrascale.pdf

OVAIS BIN USMAN (Member, IEEE) received the B.S. degree in electrical engineering from the Lahore University of Management and Sciences, Pakistan, in 2013, and the M.Sc. degree in communication systems and electronics from the Technical University of Munich, Germany, in 2015. He is currently pursuing the Ph.D. degree with Bundeswehr University Munich, Germany. His Ph.D. is focused on "on-board digital predistortion for high-throughput satellites." His research interests include the performance analysis of multiport amplifiers and 5G waveforms under non-linear power amplification in satellite specific scenarios.

ANDREAS KNOPP (Senior Member, IEEE) received the Ph.D. degree (Hons.) in radio communications from Bundeswehr University Munich, in 2008.

Since 2014, he has been a Full Professor of signal processing, coordinating in addition Germany's largest SpaceCom Laboratory and experimental satellite ground station, the Munich Center for Space Communications. Prior to taking up the faculty position, he gained expertise as a Communications Engineer and the Satellite Program Manager. His current research interests include satellite network integration and waveform design for 5G, digital satellite payloads, secure/antijam communications, and low-power mTC. He is an Entrepreneur and the Co-Founder of two start-up companies implementing his research. He is an Advisor to the German MoD, a member of the Expert Group on radio systems in the German Engineers' Association VDE/ITG, and a member of AFCEA.